Optical gain and stimulated emission in periodic nanopatterned crystalline silicon

SYLVAIN G. CLOUTIER, PAVEL A. KOSSYREV AND JIMMY XU*

Division of Engineering and Department of Physics, Brown University, Providence, Rhode Island, USA

*e-mail: Jimmy_Xu@brown.edu

Published online: 20 November 2005; doi:10.1038/nmat1530

Persistent efforts have been made to achieve efficient light emission from silicon[1–7] in the hope of extending the reach of silicon technology into fully integrated optoelectronic circuits, meeting the needs for high-bandwidth intrachip and interchip connects[8]. Enhanced light emission from silicon is known to be theoretically possible[9,10], enabled mostly through quantum-confinement effects[2–4]. Furthermore, Raman-laser conversion was demonstrated in silicon waveguides[11,12]. Here we report on optical gain and stimulated emission in uniaxially nanopatterned silicon-on-insulator using a nanopore array as an etching mask[13]. In edge-emission measurements, we observed threshold behaviour, optical gain, longitudinal cavity modes and linewidth narrowing, along with a collimated far-field pattern, all indicative of amplification and stimulated emission[14–17]. The sub-bandgap 1,278 nm emission peak is attributed to A-centre mediated phononless direct recombination between trapped electrons and free holes[18–20]. The controlled nanoscale silicon engineering, combined with the low material loss in this sub-bandgap spectral range and the long electron lifetime in such A-type trapping centres, gives rise to the measured optical gain and stimulated emission and provides a new pathway to enhance light emission from silicon.

The periodic nanopatterned silicon structure shown in Fig. 1 was fabricated by etching a highly ordered array of nanosize holes (anti-dots) into the top crystalline silicon layer of an electronic grade silicon-on-insulator (SOI) wafer. As shown in Fig. 1a, the edge emission from continuous-wave optically pumped nanopatterned samples at 10 K shows a broad emission band from 1,260 to 1,340 nm and a sharp peak at 1,278 nm, which persists up to 80 K. As shown in Fig. 1d, no such sub-bandgap emission is observed from the reference unpatterned SOI samples. The other emission bands observed at wavelengths λ below 1,250 nm are present in both patterned and unpatterned samples and are the same as reported in bulk silicon at cryogenic temperatures[21,22]. Given that the absorption length of silicon for the 514-nm excitation light is 1 μm and that the thickness of the nanopatterned-silicon layer is less than 100 nm, most of the pumping light (~90%) is transmitted down into and absorbed by the thick silicon substrate beneath the 3-μm insulator layer[8]. Therefore, these classical spontaneous photoluminescence bands ($\lambda < 1{,}250$ nm) include a large contribution from the silicon substrate, adding to the relative intensities of these emission bands when compared with the 1,278-nm emission originating from the thin nanopatterned-silicon top layer.

The 1,278-nm-peak intensity evolution with increasing incident continuous-wave pump-power is shown in Fig. 2 for different temperatures. The evolution shows a clear threshold transition from sub-threshold to linear evolution and ultimately reaches apparent saturation, which can be ascribed to heating effects at higher pump powers. Figure 2b allows a closer examination of this threshold behaviour on logarithmic scales, showing the typical superlinear (exponential) to linear transition indicative of the classical spontaneous-to-stimulated emission transition widely observed in semiconductor lasers[14,17,23]. When this transition is complete, stimulated emission dominates and the power evolution becomes linear[23]. Therefore, the observed transition behaves as expected from a system where spontaneous and stimulated emission compete[17], and is consistent with prior observations in conventional semiconductor lasers[14]. In contrast, the phonon-assisted free-exciton recombination photoluminescence band at 1,135 nm, also plotted in Fig. 2a, does not show such a transition and shows a very different power evolution, typical of pure spontaneous emission.

As shown in Fig. 3a, high-resolution spectral measurements of the 1,278-nm line show the presence of multiple peaks suggestive of the longitudinal cavity modes. The measured 96 ± 3 GHz inter-mode frequency spacing corresponds to an effective cavity optical length ($L_{\mathrm{eff}} = n_{\mathrm{eff}} \times L$) of 1.57 ± 0.05 mm. Asymmetric-waveguide modal calculations yield an average effective index $n_{\mathrm{eff}} = 1.60 \pm 0.08$ at 1,278 nm for the nanopatterned structure, including the uncertainties on the filling factor and the thickness of the top layer. Hence, the measured inter-modal spacing corresponds to a physical cavity length $L = 1.0 \pm 0.1$ mm, in good agreement with the cleaved-sample length ($L = 1.00 \pm 0.03$ mm), suggesting that the observed spectral peaks in Fig. 3a belong to longitudinal cavity modes. Moreover, as shown in Fig. 3b, the temperature evolution of the emission-peak wavelength shows the typical staircase behaviour characteristic of Fabry–Pérot resonators where the spectral position of each plateau corresponds to the five modal peaks shown in Fig. 3a.

Figure 3c compares the 1,278-nm emission line at a pumping level near threshold (12 W cm^{-2}) and well above threshold

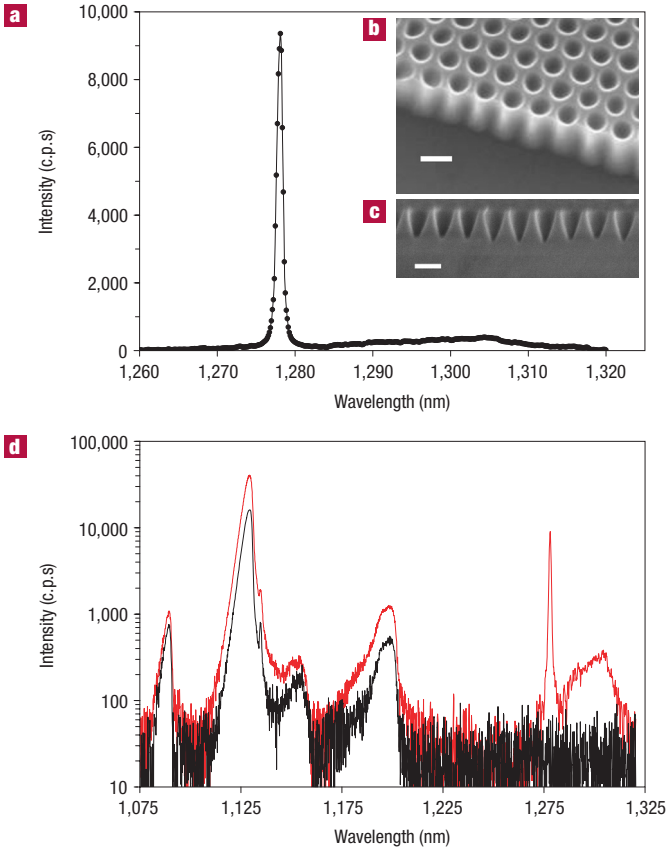

Figure 1 Edge-emission spectra and nanopatterned-silicon structure. **a**, Edge-emission spectrum from the nanopatterned SOI at 10 K. **b**, 45° view and **c**, cross-sectional view of a nanopatterned SOI sample observed under a scanning electron microscope (LEO 1530VP). The scale bars are 100 nm. **d**, Edge-emission spectra from the cleaved nanopatterned (red) and unpatterned (black) samples at 10 K.

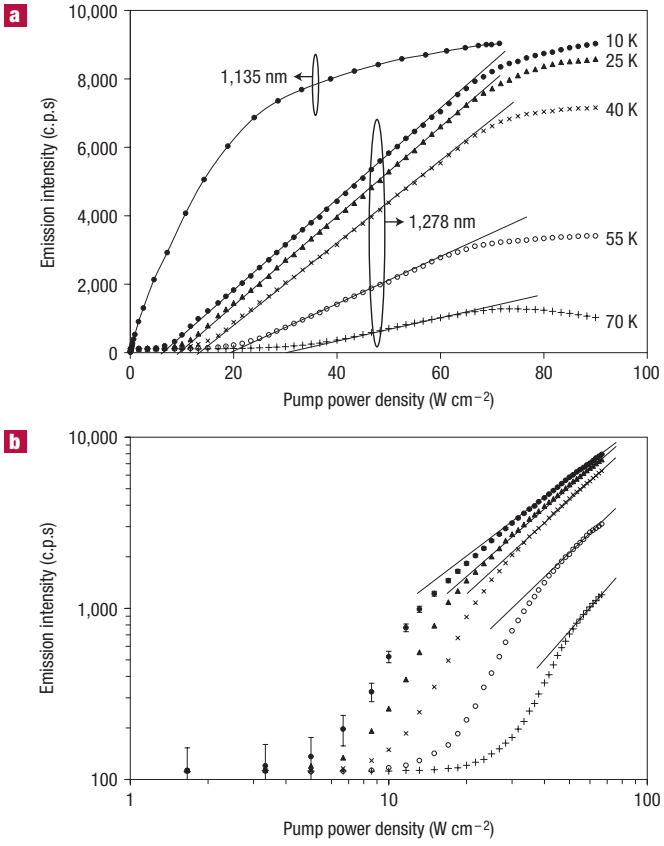

Figure 2 Evolution of the edge-emission intensity of the 1,278 nm line as a function of pump power. **a**, At fixed 10, 25, 40, 55 and 70 K temperatures. The evolution of the 1,135-nm phonon-assisted free-exciton line at 10 K is shown for comparison. Its intensity has been divided by seven to plot all curves on the same scale. **b**, Same set of 1,278 nm data shown on logarithmic scales. Error bars due to background noise are similar for all curves, but not shown for clarity.

(65 W cm^{-2}). The clear linewidth narrowing constitutes a classical signature of stimulated emission[14]. Figure 3d shows the measured linewidth as a function of the reciprocal power and shows a strong linear dependence, $\Delta\lambda = A/P + B$, where $\Delta\lambda$ is the peak spectral width and P is the pump-power density, and the fitting parameters are $A = 165 \pm 15$ cm^2 W^{-1} and $B = 0.47 \pm 0.05$ nm. Such a linear evolution with reciprocal power indicates stimulated emission as stipulated by the Schalow–Townes relation, which was theoretically predicted[24] and demonstrated in experiments[25] for semiconductor lasers.

Using the well-known variable stripe length (VSL) method[2,15], we measured the gain coefficient from the evolution of the peak-emission intensity as a function of the optically pumped sample length. The linear region shown in Fig. 4a on semi-logarithmic scales represents the expected exponential increase of intensity associated with the increasing length of the optically pumped section[2,15,16,26]. The net optical-gain coefficient, defined as $G = \Gamma g - \alpha$ (where Γ is the modal confinement factor, g is the material gain and α is the overall waveguide loss coefficient[26]), can be directly obtained from the slope of this linear region. The net optical-gain coefficients so measured are 260, 247, 230, 165 and 88 ± 5 cm^{-1} at 10, 25, 40, 55 and 70 K, respectively, when the excitation pump-power density was set at 65 W cm^{-2}. When the pump-power density was reduced to 8 W cm^{-2} under otherwise identical experimental conditions, the net optical-gain coefficient measured at 10 K and obtained from the data fitting becomes negative (-31 ± 5 cm^{-1}) and is dominated by propagation losses[26–28]. The transition from a negative to a positive gain coefficient constitutes another classical indicator of stimulated emission[27,28]. For the purposes of setup validation, we also measured the optical-gain coefficients from bulk gallium arsenide (GaAs) samples using the same VSL configuration, and we obtained values in agreement with literature reports.

At first, the measured optical-gain coefficients may seem surprisingly large. However, as shown in Fig. 4a, the optical gain starts saturating for excited lengths longer than 100–200 μm depending on the sample temperature, as expected from any finite power-supply amplification process[2,15,26]. Therefore, the total amplification factor remains reasonable owing to the relatively short saturation length, even though the net gain coefficients seem to be unexpectedly large. One may compare these results with reports on optical gain using silicon nanocrystals embedded in silica waveguides[2]. In ref. 2, smaller gain coefficients (~110 cm^{-1}), which were partly owing to the higher propagation losses (41.5 cm^{-1}) in the higher photon-energy range[27,28], associated with longer saturation lengths (~250 μm), resulting in similar total amplification factors to those we report in our system, were measured at room temperature using the same VSL technique.

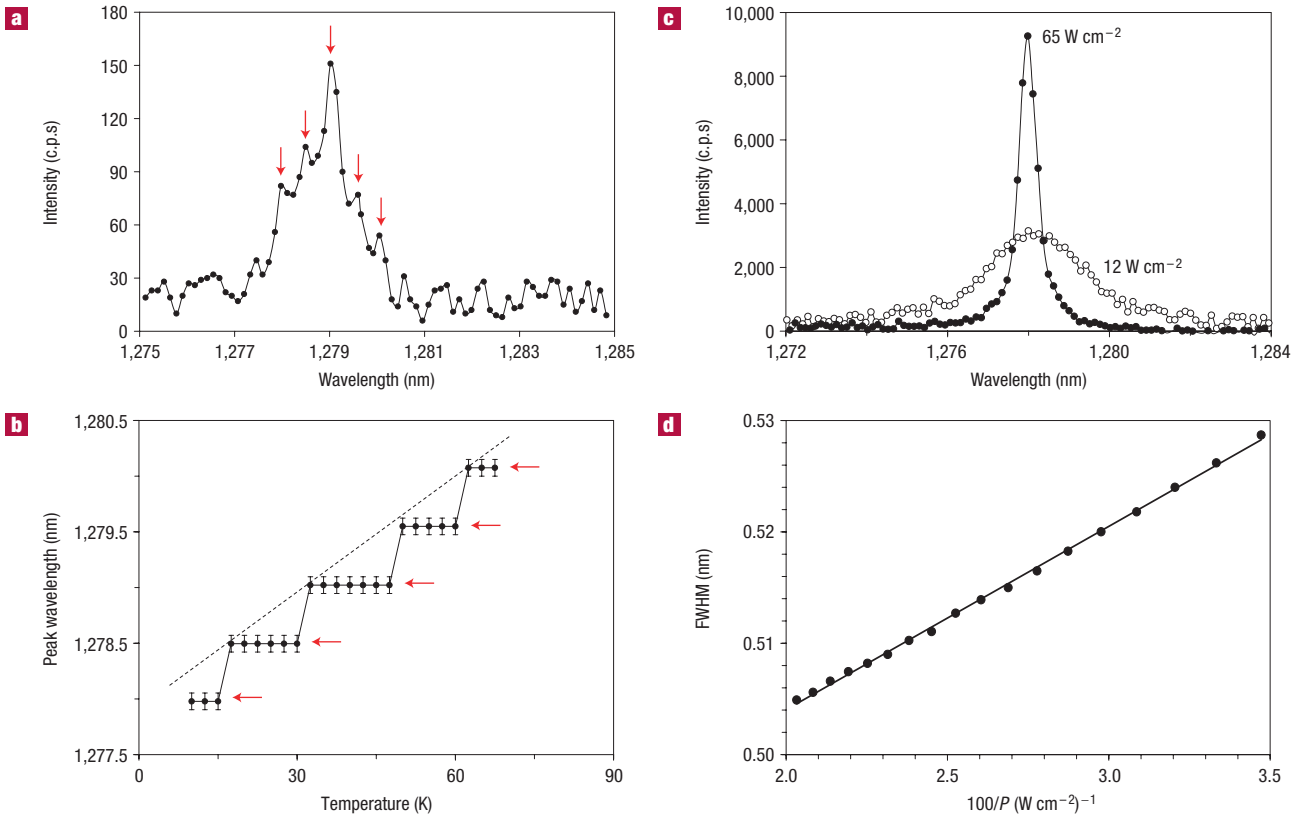

Figure 3 Spectral features of the 1,278-nm edge-emission line. a, Typical high-resolution spectrum measured at 40 K. **b**, Evolution of the peak wavelength as a function of temperature. The error bars (standard deviation) define the spectral accuracy range. **c**, Comparison of the emission spectra at 12 and 65 W cm^{-2} pump-power densities. The intensity of the 12 W cm^{-2} spectrum was multiplied by three to allow comparison. **d**, Spectral width evolution with reciprocal pump power at 10 K.

Finally, we measured the far-field intensity distribution of the gain-guided edge emission. In the direction normal to the silicon film, the far field is expected to diverge because of the extremely thin active layer. In the lateral direction, the measured far-field distribution shown in Fig. 4b and c shows a 1.1 ± 0.1 degree collimation, as expected for spatially coherent emission from a wide and thin stripe of active material[23]. The efficiency of the 1,278 nm emission is expected to be low in this unoptimized sample structure, and is further lowered by extrinsic factors such as the broad-area pumping, ultra-thin ($\leq$100 nm) active layer, asymmetric waveguiding and pump laser-induced heating effects. Indeed, the external efficiency of the 1,278 nm emission measured at 10 K is in the range of 10^{-6}–10^{-5}, at the output power level of 30 ± 5 nW. Even though the external efficiency may seem to be very low, it is comparable to the optically pumped solid-state lasers in their early days[29] ($\sim 10^{-6}$) and conventional noble-gas lasers[17] ($\sim 10^{-5}$), and is indicative of the great room for future improvements.

Although these experimental observations strongly suggest that significant optical gain and stimulated emission can be achieved in periodic nanopatterned crystalline silicon, a complete understanding or analysis of the observed phenomena is not readily available at this early stage. However, a few key elements of the enhanced radiative transitions can already be identified. For one, the sub-bandgap emission at 1,278 nm can be attributed to the so-called A-centre mediated radiative recombination[18,19]. It has been established that an A-centre defect state, located 0.17 eV below the conduction band edge of silicon, allows direct (phononless) recombination between trapped electrons and free holes[18]. The exact nature and origin of the A-type trapping centres have remained a subject of inquiry[20], but are more often attributed to silicon vacancies[18,19]. Observations of such bands in γ-ray irradiated silicon unexposed to any further chemical treatment apparently excludes chemical contaminants as a possible origin[18]. In our system, the periodic anti-dots can be viewed as controllably created nanoscopic zones of high-density A-centre states. The measured 34 ± 5 meV process activation energy for the 1,278 nm line, in good agreement with other reports[20], provides further support for the A-centre hypothesis. One can reason that with a sufficiently long electronic lifetime in such trapped states, population-inversion conditions can be established in this three-level system[18], similarly to the proposed process for silicon nanocrystals embedded in silica waveguides[2]. Further possible factors such as localized strain, local symmetry breaking, or exciton localization and condensation around the anti-dots may also play a role and remain open to further investigation. Although reminiscent of periodic photonic bandgap structures, the 110 nm period is fourfold to fivefold too small to invoke photonic bandgap effects for the 1,278 nm emission wavelength[30]. Therefore, wave propagation in this silicon nanostructure is unlikely to depend on the long-range order of the anti-dots or their diameter, whose effect is mostly a weak Rayleigh scattering. This was confirmed by the observation of similar emission properties from structures with different periodicities and pore sizes, and using various excitation wavelengths.

Evidence of light amplification and stimulated emission was clearly observed in the edge-emission measurements from nanoengineered crystalline silicon. Although only observed at cryogenic temperatures so far, we hope this report will help

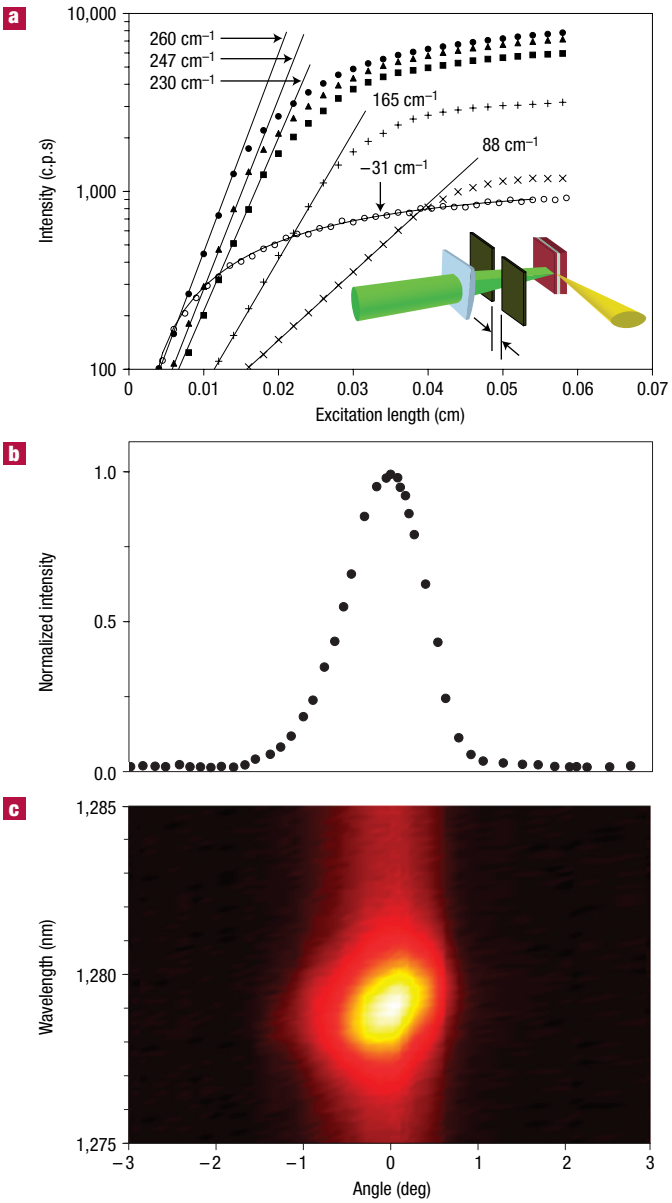

Figure 4 Optical gain at 1,278 nm and lateral far-field pattern. a, Evolution of the edge-emission intensity as a function of the optically pumped sample length for a 65 W cm^{-2} pump-power density at 10, 25, 40, 55 and 70 K corresponding to 260, 247, 230, 165 and 88 $\pm$ 5 cm^{-1} net optical-gain coefficients respectively. Measurement at 10 K and 8 W cm^{-2} pump-power density is shown for comparison and yields a negative (-31 ± 5 cm^{-1}) gain coefficient dominated by propagation losses. Inset: Illustration of the VSL measurement method. **b**, 1,278 nm lateral far-field intensity pattern and **c**, lateral far-field intensity distribution versus wavelength at 10 K.

generate broad interest and stimulate further investigations in theory and experiments, enabling a better understanding of the underlying mechanisms, improved performance, operation at higher temperatures and electrical pumping.

METHODS

SAMPLE FABRICATION

The original SOI wafer from SOITEC has a 205-nm-thick undoped silicon ⟨100⟩ layer separated from the thick silicon substrate by 3 μm of silicon-oxide insulator. The top layer was further thinned to a 80 $\pm$ 20 nm thickness by means of thermal oxidation followed by highly selective wet-etching of the oxidized silicon in HF-based solution. The high uniformity in the nanopatterning is enabled by the use of an anodic aluminium oxide (AAO) nanopore membrane as an etching mask. The 750-nm-thick AAO mask was fabricated using a two-step aluminium anodization process, in which uniform 60-nm-wide nanopores form and self-organize into a periodic array[13], and was placed atop the thinned SOI. The nanopore pattern was transferred into silicon using conventional chlorine-based reactive-ion etching. Subsequently, the AAO mask was removed. This technique allows uniform nanopatterning over a large area (~1 cm^2). The samples used for experiments had resultant cone-shaped pores with 110-nm centre-to-centre spacing. 1.00 $\pm$ 0.03-mm-wide slivers of such patterned SOI were cleaved for edge-emission measurements and compared with cleaved unpatterned thinned SOI. To minimize material loss, we used undoped crystalline SOI, therefore requiring optical pumping.

EDGE-EMISSION MEASUREMENTS

Samples were loaded in a cryostat and a continuous-wave 1.5 W argon-ion pump laser at 514.5 nm was magnified and then focused onto the sample's top surface using a $f = 4$ cm cylindrical lens so that the pump-power density was uniform across the entire excited area. The excitation area was measured to be a long stripe of 100 $\pm$ 50 μm width exciting the entire sample length (1.00 $\pm$ 0.03 mm). The edge emission was collected using a long focal length ($f = 30$ cm) and large diameter (7.5 cm) concave mirror and focused on the entrance slit of a Horiba TRIAX spectrometer through a long-pass filter blocking all background light at wavelengths below 980 nm. The spectrometer is equipped with a thermo-electrically cooled InGaAs diode-array photodetector. For the measurements shown in Fig. 1, the sample temperature was 10 K and the pump-power density was 65 W cm^{-2}, uniform over the excited area ($1.0 \pm 0.5 \times 10^{-3}$ cm^2). Several excitation wavelengths from 456 to 808 nm were used leading to identical sub-bandgap emission spectra.

For the measurements shown in Fig. 2, the same excitation and collection configuration was used and the pump-power density was continuously varied up to 95 W cm^{-2} for different fixed sample temperatures (10, 25, 40, 55 and 70 K).

For the measurements of Fig. 3a and b, the spectrometer entrance slit was narrowed down to 0.05 mm to allow high spectral resolution and the excitation power was set to 75 W cm^{-2} in the same configuration as described to compensate for the low emission coupled to the spectrometer through the narrow entrance slit. For the specific spectrum shown in Fig. 3a, the sample temperature was set to 40 K and for the temperature evolution shown in Fig. 3b, it was continuously varied from 10 to 70 K with an accuracy of $\pm$0.5 K. For the measurements of Fig. 3c and d, the spectrometer entrance slit width was increased to allow high detection sensitivity near threshold.

GAIN MEASUREMENTS

In the same pumping and collection configurations, a variable slit was placed ~2 cm from the sample's top surface to controllably change the sample's optically excited length. The minimum distance of the slit was limited by the cryostat chamber dimensions. The excitation power density was set to 65 and 8 W cm^{-2}. The edge emission was collected and focused on the entrance slit of the spectrometer as described. We verified that coupling effects were minimized[26] by scanning the sample length with a circular (150-μm-diameter) excitation spot of identical power density (65 W cm^{-2}). Accordingly, the measured fluctuation of the detected intensity was less than 5%. Finally, to evaluate the influence of possible slit diffraction effects on the uniformity of the pump[26,27] and for the sake of comparison, we used both a rectangular variable slit and a shadow mask as used in refs 2,15. The gain coefficients measured with both slit configurations agree within 10%, suggesting that diffraction effects can also be safely disregarded.

LATERAL FAR-FIELD INTENSITY-DISTRIBUTION PATTERN

In the same pumping configuration, the excitation power was set to 70 W cm^{-2} over the entire sample length. The edge emission at 10 K was collected through a scanning slit and measured using the spectrometer as described.

RAMAN SPECTROSCOPY AND LASER HEATING

To evaluate pump laser-induced heating effects in the samples, we used a ThermoNicolet Almega Dispersive-Raman microscope. Using a 532 nm excitation laser (close to the 514 nm excitation used in this work) and a ~100 W cm^{-2} excitation power, we measured a cross-sectional laser-induced heating of 10.2 $\pm$ 0.4 K in the original unpatterned SOI and 11.6 $\pm$ 0.4 K in the nanopatterned SOI at room temperature.

Received 23 May 2005; accepted 11 October 2005; published 20 November 2005.

References

1. Pavesi, L., Gaponenko, S. & Dal Negro, L. *Towards the First Silicon Laser* (Kluwer Academic, Dordrecht, 2003).
2. Pavesi, L., Dal Negro, L., Mazzoleni, C., Franzo, G. & Priolo, F. Optical gain in silicon nanocrystals. *Nature* **408,** 440–444 (2000).
3. Wilson, W. L., Szajowski, P. F. & Brus, L. Quantum confinement in size-selected surface-oxidized silicon nanocrystals. *Science* **262,** 1242–1244 (1993).
4. Lu, Z., Lockwood, D. J. & Baribeau, J. Quantum confinement and light emission in SiO_2/Si superlattices. *Nature* **378,** 258–260 (1995).
5. Green, M. A., Zhao, J., Wang, A., Reece, P. J. & Gal, M. Efficient silicon light-emitting diodes. *Nature* **412,** 805–808 (2001).
6. Ng, W. L. *et al*. An efficient room-temperature silicon-based light-emitting diode. *Nature* **410,** 192–194 (2001).
7. Chen, M. J. *et al*. Stimulated emission in nanostructured silicon pn junction diode using current injection. *Appl. Phys. Lett.* **84,** 2163–2165 (2004).
8. Salib, M. *et al*. Silicon photonics. *Intel. Tech. J.* **8,** 143–160 (2004).
9. Landsberg, P. T. Radiative decay in compound semiconductors. *Solid State Electron.* **10,** 513–537 (1967).
10. Trupke, T., Green, M. A. & Würfel, P. Optical gain in materials with indirect transitions. *J. Appl. Phys.* **93,** 9058–9061 (2003).
11. Boyraz, O. & Jalali, B. Demonstration of a silicon Raman laser. *Opt. Express* **12,** 5269–5273 (2004).
12. Rong, H. *et al*. An all-silicon Raman laser. *Nature* **433,** 292–294 (2005).
13. Liang, J., Chik, H., Yin, A. & Xu, J. Two-dimensional lateral superlattices of nanostructures: Nanolithographic formation by anodic membrane template. *J. Appl. Phys.* **91,** 2544–2546 (2002).
14. Quist, T. M. *et al*. Semiconductor maser of GaAs. *Appl. Phys. Lett.* **1,** 91–92 (1962).
15. Shaklee, K. L., Nahory, R. E. & Leheny, R. F. Optical gain in semiconductors. *J. Lumin.* **7,** 284–309 (1973).
16. Dingle, R., Shaklee, K. L., Leheny, R. F. & Zetterstrom, R. B. Stimulated emission and laser action in gallium nitride. *Appl. Phys. Lett.* **19,** 5–7 (1971).
17. Siegman, A. E. *Lasers* (University Science Books, Susalito, 1986).
18. Spry, R. J. & Compton, W. D. Recombination luminescence in irradiated silicon. *Phys. Rev.* **175,** 1010–1020 (1968).
19. Yukhnevich, A. V. The structure of the spectrum of the radiative capture of holes by A-centers in silicon. *Sov. Phys. Solid State* **7,** 259–261 (1965).
20. Jones, C. E., Johnson, E. S., Compton, W. D., Noonan, J. R. & Streetman, B. G. Temperature, stress, and annealing effects on the luminescence from electron-irradiated silicon. *J. Appl. Phys.* **44,** 5402–5410 (1973).
21. Pokrovskii, Y. Condensation of non-equilibrium charge carriers in semiconductors. *Phys. Status Solidi A* **11,** 385–410 (1972).
22. Vouk, M. A. & Lightowlers, E. C. Two-phonon assisted free exciton recombination radiation from intrinsic silicon. *J. Phys. C* **10,** 3689–3698 (1977).
23. Suematsu, Y. & Adams, A. R. *Handbook of Semiconductor Lasers and Photonic Integrated Circuits* (Chapman and Hall, London, 1994).
24. Henry, C. H. Theory of linewidth of semiconductor lasers. *IEEE J. Quantum Electron.* **18,** 259–264 (1982).
25. Fleming, M. W. & Mooradian, A. Fundamental line broadening of single-mode (GaAl)As diode lasers. *Appl. Phys. Lett.* **38,** 511–513 (1981).
26. Dal Negro, L., Bettotti, P., Cazzanelli, M., Pacifici, D. & Pavesi, L. Applicability conditions and experimental analysis of the variable stripe length method for gain measurements. *Opt. Commun.* **229,** 337–348 (2004).
27. Dal Negro, L. *et al*. Stimulated emission in plasma-enhanced chemical vapour deposited silicon nanocrystals. *Physica E* **16,** 297–308 (2003).
28. Ruan, J., Fauchet, P. M., Dal Negro, L., Cazzanelli, M. & Pavesi, L. Stimulated emission in nanocrystalline silicon superlattices. *Appl. Phys. Lett.* **83,** 5479–5481 (2003).
29. Johnson, L. F., Boyd, G. D., Nassau, K. & Soden, R. R. Continuous operation of a solid-state optical maser. *Phys. Rev.* **126,** 1406–1409 (1962).
30. Lupu, A. *et al*. Experimental evidence for superprism phenomena in SOI photonic crystals. *Opt. Express* **12,** 5690–5696 (2004).

Acknowledgements

We acknowledge the timely and enabling support from ONR and DARPA. S.G.C. and J.X. are also grateful to NSERC and the Guggenheim Foundation, respectively, for the fellowship support.
Correspondence and requests for materials should be addressed to J.X.

Competing financial interests

The authors declare that they have no competing financial interests.